



## Modeling of Variational Gradient Porous Architecture with Multi-directional Filament Deposition in 3D Scaffolds

AKM Khoda<sup>1</sup>, Ibrahim T. Ozbolat<sup>2</sup> and Bahattin Koc<sup>\*3</sup>

<sup>1</sup>University at Buffalo, [akm32@buffalo.edu](mailto:akm32@buffalo.edu)

<sup>2</sup>The University of Iowa, [ibrahim-ozbolat@uiowa.edu](mailto:ibrahim-ozbolat@uiowa.edu)

<sup>3</sup>Sabanci University, Istanbul, [bahattinkoc@sabanciuniv.edu](mailto:bahattinkoc@sabanciuniv.edu)

### ABSTRACT

Porous scaffolds with interconnected and continuous pores have recently been developed to stimulate tissue regeneration. Even though few researches have focused on the internal architecture of porous scaffolds but concluded that properly interconnected and continuous pores with spatial distribution might perform diverse mechanical, biological and chemical functions of a scaffold. Thus the need for reproducible and fabricatable scaffold design with controllable gradient porosity is obvious but is hardly achieved because of design and fabrication limitations. In this paper, a novel functionally gradient variational porosity architecture has been proposed with continuous material deposition planning scheme. The medial axis transformation for the scaffold has been calculated to generate an internal feature of the geometric domain. The medial axis is then used as a base to develop the medial boundary to define the medial regions. Then the complex internal architecture of scaffolds is divided into sub-regions using the ruling lines that are generated between the slice contour and the medial boundary. The desired controlled variational porosity along the scaffold architecture has been achieved with the combination of two geometrically oriented consecutive layers while meeting the tissue scaffold design constraints. This ensures truly porous structures in every direction as well as controllable porosity with interconnected pores along the scaffold architecture. The proposed methodology has been implemented and illustrative examples are also provided. A sample designed structure has been fabricated with a NC motion controlled micro-nozzle deposition system.

**Keywords:** medial axis, variational porosity, internal scaffold architecture.

**DOI:** 10.3722/cadaps.2013.445-459

## 1 INTRODUCTION

To stimulate the guided tissue regeneration and expedite the wound healing process, researchers tried to use porous structures to deliver bio-molecules (usually cytokines) and/or cells to the damaged tissue area. One major purpose for using such porous structure is to induce amenable bio-reactor in the tissue regeneration site and to protect the seeded cell/ bio-molecules against host immunorejection [13] and thus stimulating the healing process. Such carrier structures, known as scaffolds, require a multi-variable objective function incorporating build materials, bio-compatibility, degradability, permeability, surface chemistry, mechano-biological properties, pore size, porosity, fabrication technology and internal architecture.

A fundamental scaffold design expectation in tissue engineering is that the degradation of scaffold material and new tissue formation occur simultaneous [1], i.e. scaffold act as extra cellular matrix (ECM) to support cell proliferation while remain viable to the end of the healing phase and then fully absorbed. But the current design strategies have failed to attain such delicate equilibrium and thereby missing the goal for successful tissue regeneration. Most of the developed three-dimensional scaffolds demonstrated limited tissue ingrowth due to restrained nutrient supply imposed by intrinsic geometrical and structural characteristics. Such spatially insufficient nutrient and oxygen supply limits the cell adhesion on the surface of the scaffold and prevent their homogeneous migration [18]. A successful design of scaffolds involves comprehensive consideration of both macro and micro-structural properties of the scaffolds and their interactions with natural tissue. Such interactions are very much dependent upon the scaffold's internal architecture. The internal architecture should be repeatable, fully integrated, complex, three-dimensional, and controlled porous structures which conform the anatomical shape and size of the replacement of tissue or organs [6].

Toward development of an ideal carrier/scaffold, researchers are mainly aiming at material types and properties, their processing conditions and biological compatibility [12, 15] to quantify its functionality. Even though the internal architecture of a scaffold may have significant influence on the cellular microenvironment, few researches have focused on the internal architecture of the porous scaffold and even fewer have tried to optimize the scaffold's geometric structure. Such design as well as fabrication limitations forced researcher to use homogeneous scaffolds with uniform pore size fabricated with solid free-form fabrication (SFF) processes [8]. But the desired choreographed multi-functionality of scaffold may only be achieved with optimally designed biodegradable carriers with properly interconnected pores and controllable spatial material distribution [1, 14]. Moreover homogeneous scaffolds do not capture the intricate spatial material concentration and may not represent the bio-mimetic structure of the regenerated tissue. Gradient porosity along the internal scaffold architecture might provide extrinsic and intrinsic properties of scaffolds. A possible solution for performing the diverse functionality would be designing scaffolds with functionally variational porosity. Thus achieving controllable, continuous, interconnected gradient porosity with reproducible and fabricatable design may lead toward a successful tissue engineering approach.

In this paper, we propose a novel method to design functionally gradient porosity architecture which conforms the anatomical shape of the damaged tissue and maintains the continuity with connectivity.

## 2 METHODOLOGY

To model the scaffold, the anatomical 3D shape of the targeted damaged area need to be extracted using non-invasive techniques. Firstly, medical image obtained from Computed Tomography (CT) or Magnetic Resonance Imaging (MRI) is used to get the geometric and topology information of the

replaced tissue/organs. The initial geometric information of the model is represented as a mesh or Stereolithography (STL) model. The STL files are generated by tessellating the outside surface of the object with triangles. The 3D tissue models are then sliced by a set of intersecting planes parallel to each other to find the slice contours. The contours are generated by connecting the intersection points between the planes and the surface and are suitable for a SFF based processes. All the contour curves are simple planar closed curves i.e. they do not intersect themselves other than their start and end points and have the same (positive) orientation. The general equation for these contours can be parametrically represented as:

$$\begin{aligned} C_i(t_i) &= (x(t_i), y(t_i)) \quad \forall i = 0, \dots, m \\ t_i &\in [a_i, b_i] \\ C_i(a_i) &= C_i(b_i) \end{aligned} \quad (2.1)$$

Here,  $C_i(t_i)$  represent the parametric equation for  $i^{\text{th}}$  contour with respect to parameter  $t_i$  at a range between  $[a_i, b_i]$ . The distance between the intersecting planes can be constant in uniform slicing or varying height for non- uniform slicing. The consecutive slices i.e.  $i^{\text{th}}$  and  $(i+1)^{\text{th}}$  are discretized by multi-directional zigzag pattern and concentric spiral like pattern respectively and the methodology is applied and demonstrated on the pair slice geometry based on the designed porosity.

## 2.1 Medial Axis Construction

Because of the nature of the tissue scaffold and its functionality, we decided to introduce an internal feature of the scaffold region. Such internal feature can be used as a base for discretizing the internal architecture with proper directional uniformity. Medial axis (MA) [2] which is a symmetric bisector will be used as the internal features.

A medial-axis,  $M_i(C_i)$  in this paper has been generated for every planar closed contour or slice  $C_i$  using offsetting as shown in Fig 1(a). The approximated offset curve  $C_i^d(t_i)$  of the contour curve  $C_i(t_i)$  at a distance  $d$  from the boundary is defined by:

$$C_i^d(t_i) = C_i(t_i) + d\vec{N}(t_i) \quad (2.2)$$

Where  $\vec{N}(t_i)$  is the unit normal vector on curve  $C_i(t_i)$  at a parametric location  $t_i$ . Such offset may generate self-intersection if  $d$  is larger than minimum radius of curvature at any parametric location  $t_i$ . Such intersections during offsetting have been eliminated by implementing the methodology discussed in our earlier work [11]. A singular point is obtained at each self-intersection event where there is no  $C^1$  continuity. Medial axis segments are generated by obtaining the intersection of each offset curves and then by connecting them together as piecewise linear curve. Any branch point for medial axis in this paper is assumed to be located at the center of loci that is tangent to three boundaries simultaneously. The branch connection has been determined by higher offset resolution and interpolation as discussed in Ozbolat et al [16].

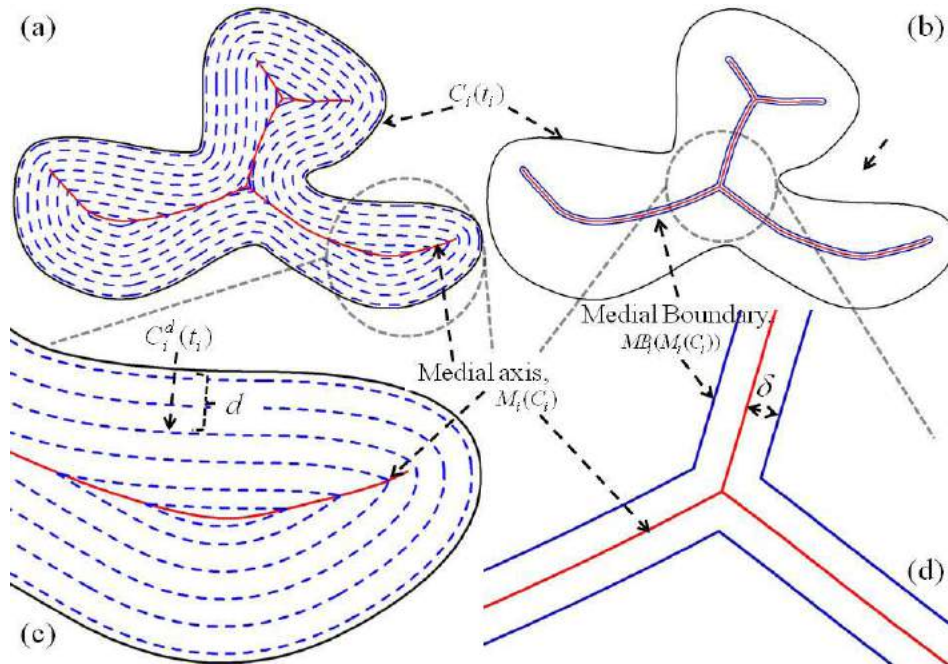


Fig. 1: (a) The medial axis generation, (b) medial boundary, (c) and (d) corresponding zoomed view.

## 2.2 Generating Ruling Lines

To generate porous structure, the designed scaffold needs to be divided with finite number of segments by drawing lines between the slice contour  $C_i$  and its corresponding medial axis  $M_i(C_i)$ . The easiest way to construct such lines is to divide both curves either with equal number of equidistant points or by parametrically connecting the points between them. To avoid self-intersecting segments, a feature matching ruling lines technique [9] based on a dynamic programming is used. It is assumed that a medial region is always a closed curve. A medial boundary,  $MB_i(M_i(C_i))$  curve is constructed for  $i^{th}$  slice by offsetting medial axis (MA) in both inward and outward directions with a distance  $\delta$  :  $ll' \leq 2\delta \leq ul'$  where  $ul'$  and  $ll'$  represent upper and lower width for allowable pore size as shown in Fig 1(b). The width of this medial boundary channel  $\delta$  can be adjusted based on the required biological functionality [3]. Any self intersection points or loops of the calculated offset curves are then removed with the same methodology discussed in [11]. At the end of the process, a closed, planner medial boundary is generated.

Both contour curve  $C_i(t_i)$  and medial boundary,  $MB_i(M_i(C_i))$  curve are parametrically divided into  $n_1$  and  $n_2$  independent finite number of sections with a set of points  $P_{C_i} = \{p_{c_i,j}\}_{j=0,1..n_1}$  and  $P_{MB_i} = \{p_{MB_i,k}\}_{k=0,1..n_2}$  respectively. The developed dynamic programming uses distance based optimization between the feature point set  $\|P_{C_i}, P_{MB_i}\|$  for matching with singularity and connecting the ruling lines. Both over-connectivity and zero-connectivity with those point sets are addressed with the same methodology discussed in our earlier paper [9]. Thus the proposed methodology generates at

least  $n$  number of uninterrupted ruling lines,  $RL = \{rl_n\}_{n=\max\{n_1, n_2\}}$  between contour curves and their corresponding medial boundaries.

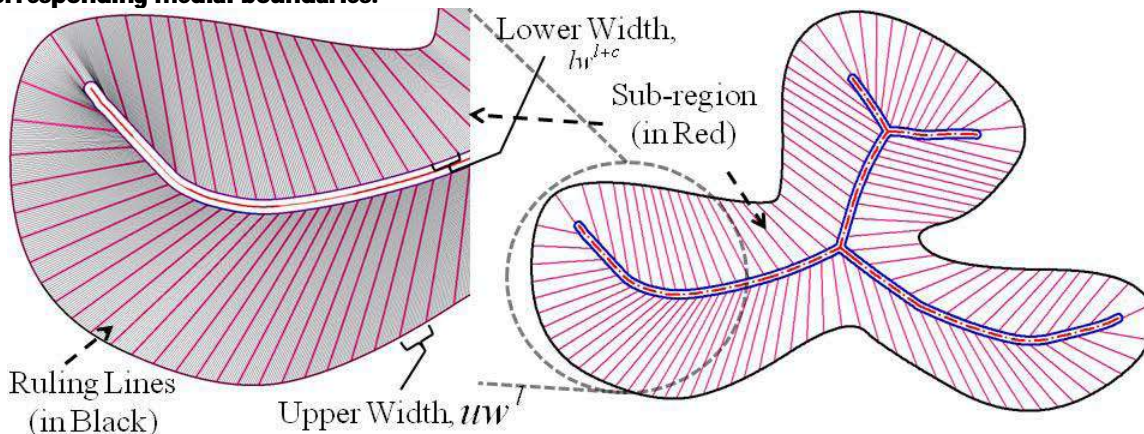


Fig. 2: Sub-region formation from ruling lines.

### 2.3 Area Accumulation into Sub-regions

Internal area of the scaffold is segmented into sub-regions with equal area by accumulating the segments between the ruling lines as shown in Fig 2. Such sub-regions can be considered as channels between the contour and the medial boundary which is the deepest region and must satisfy the biological requirement i.e. nutrient, fluid and oxygen flow. Thus the sub-region accumulation is considered as an optimization problem with constraint that ensures functional requirements and uniformity. The following minimization problem [9] is solved to achieve the set of sub-regions,  $S = \{s_l\}_{l=0,1\dots L}$  where  $l$  is the number of feasible sub-regions.

$$\text{Min } \sum_l (S_0^{Area} - S_l^{area}) \quad \forall l \quad (2.3)$$

Subject to-

$$ll \leq lw^l \leq ul \quad \forall l \quad (2.4)$$

$$ll \leq uw^l \leq ul \quad \forall l \quad (2.5)$$

$$\sum_l S_l^{area} \approx \dot{A} \quad (2.6)$$

$$S_m \cap S_n = \emptyset \quad \forall m \text{ and } n = 0\dots l \quad (2.7)$$

Here,  $S_0^{area}$  is user-defined acceptable constant sub-region area;  $S_l^{area}$  is the  $l^{\text{th}}$  sub-region area;  $lw^l$  and  $uw^l$  are the lower and upper widths respectively,  $\dot{A}$  is the total area. The parameters  $ul$  and  $ll$  represent the upper and lower limit for allowable sub-region widths which satisfy the biological and fabrication requirements. In the literature [4, 7] the range for lower width has been suggested as 100  $\mu\text{m}$  - 350  $\mu\text{m}$  for hard tissue and 30  $\mu\text{m}$  - 150  $\mu\text{m}$  for soft tissue. For upper width, even a wider range of 200  $\mu\text{m}$  - 900  $\mu\text{m}$  has been suggested. Eqn. (2.7) ensures that the sub-regions do not intersect with each other.

## 2.4 Decomposing the Sub-regions on Medial Axis

The generated sub-regions are multi-directional and their alignment depends upon the outer contour profile and ruling line density. Moreover, the sub-regions are constructed in a way that the sets are mutually exclusive and collectively exhaustive, i.e. they share arms with the adjacent neighboring sub-region. Therefore, each sub-region is basically separated from its adjacent neighbor by the sub-region arm  $SA = \{SA_i\}_{i=0,1,\dots,L}$  where  $SA \subseteq RL$  and are generated by the algorithm presented in Section 2.3. Thus the generated sub-region sets can be represented with two end points,  $SP = \{sp_i\}_{i=0,1,\dots,L}$  and  $BP = \{bp_i\}_{i=0,1,\dots,L}$  of the corresponding arm. Here,  $sp_i$  and  $bp_i$  are the starting points on the contour curve and the medial boundary respectively as shown in Fig. 3.

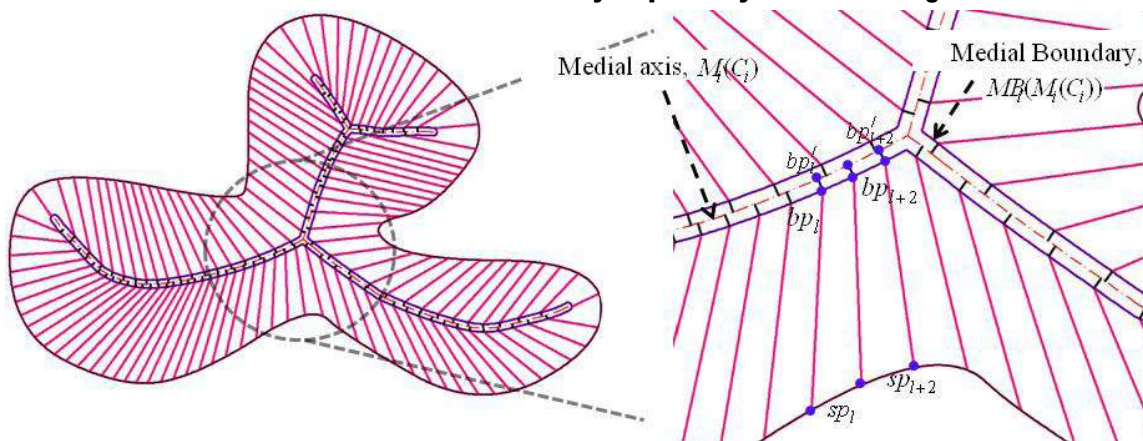


Fig. 3: Decomposing of sub-region base on medial axis.

As discussed earlier, the medial region (channel) is located as the skeleton of the layer and might be used as internal perfusion channel through which the cell nutrient and oxygen can be supplied and thus can increase the cell survival rate. But the presence of this feature separates the scaffolding area and their corresponding sub-regions as shown in Fig. 2. In other words, the sub-regions arm set  $SA$  are cut through by the Medial Boundary which makes the medial region a long channel. To ensure the structural integrity along the medial region and the overall stability of the scaffold architecture, the point set  $BP$  for all sub-regions need to be projected over the medial axis along the direction  $\vec{N}_i(bp_i)$  which would create a new point set  $BP' = \{bp_i'\}_{i=0,1,\dots,L}$ . Here,  $\vec{N}_i(bp_i)$  is the unit normal vector on the medial boundary  $MB(bp_i)$  at  $bp_i$  and  $bp_i'$  is the projected point location as shown in Fig. 3. Such methodology brings the lower width for each sub-region onto the medial axis base and connects the sub-regions arms from the other side of the medial axis. The projecting lines then divide the long medial region into suitable pores ensuring both biological and mechanical functionalities. Accumulation of these sub-region sections ends the design process for the first layer and become the support base for the second layer to achieve the variational and interconnected porosity architecture.

## 2.5 Determining Porosity by Dividing Sub-regions

The layer generated with the accumulated sub-regions conforms to the biological functionality for such scaffold structure with the constraints applied during the accumulation process with Eqn. (2.3)-(2.7). But building the whole structure only using the sub-regions would significantly reduce the

connectivity within the scaffolding area as well structural integrity since this will build a solid wall rather than a porous boundary. To ensure a truly porous structure in every direction as well as controllable porosity with interconnected pores along the scaffold architecture, the successive layer has been designed by virtually discretizing the sub-regions along its peripheral.

To generate the pores on the scaffold, each equal area sub-regions have been divided according to area across their arms as shown in Fig 4 (a). These segments of each sub-section are considered as pore cells,  $PC_l^m$  of the scaffold. Because of the free-form shape of the outer contour and the accumulation pattern, the generated sub-regions have highly anisotropic shapes which eventually generates anisotropic pore cell. The following algorithm has been used to divide the sub-regions.

$$\text{Min} \sum_{m=0}^M |PC(m) - PC_l^m| \quad \forall \quad 0 \leq l \leq L \tag{2.8}$$

Subject to-

$$\frac{S_0^{area}}{\max\_PC} \leq M \leq \frac{S_0^{area}}{\min\_PC} \tag{2.9}$$

$$\sum_{m=0}^M PC_l^m = S_l^{area} \quad \forall \quad 0 \leq l \leq L \tag{2.10}$$

$$PC_x^m = PC_y^m \quad \forall \quad 0 \leq m \leq M, \quad 0 \leq x, y \leq L \tag{2.11}$$

This minimization problem is used to reduce the deviation from the desired or expected pore cell area,  $PC(m)$  with the generated pore cell area,  $PC_l^m$ . Here,  $\max\_PC$  and  $\min\_PC$  denotes the maximum and minimum allowable pore cell areas respectively. In literature, the designed pore cells are usually uniform shape. Since the generated pores are anisotropic, an allowable range of pore cell areas needs to be used [9]. The total number of pore cells in every single sub-region need to be the same to ensure continuous fabrication as represented in Eqn. (2.10). Moreover a pore cell sharing the same location in any sub-regions has equal area and within the allowable size as ensured by Eqn. (2.11).

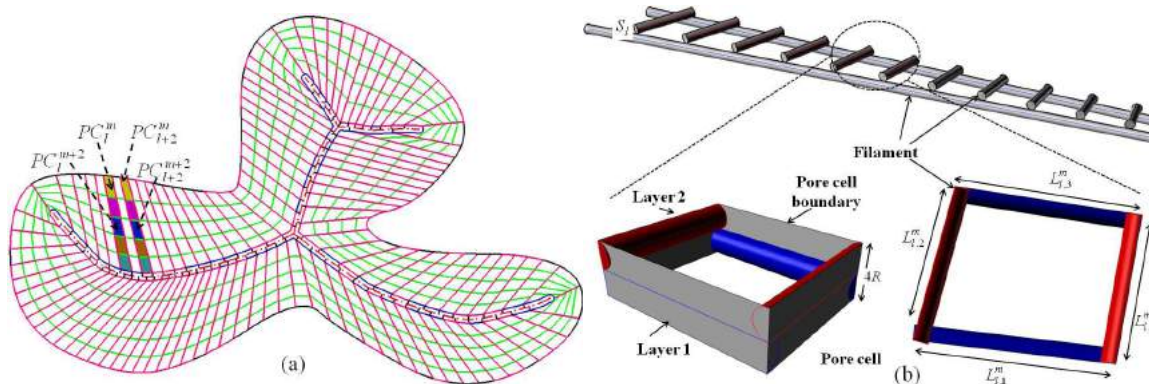


Fig. 4: (a) Dividing the sub-regions to generate pore cell (b) porosity calculation for anisotropic pore cell.

The porosity for the generated anisotropic pore cell can be measured by the following equation-

$$\%Porosity_l^m = 1 - \frac{(L_{l,1}^m + L_{l,2}^m + L_{l,3}^m + L_{l,4}^m) \times \pi \times R^2}{Area - L_{l,1}^m L_{l,2}^m L_{l,3}^m L_{l,4}^m \times 8 \times R} \quad \forall l, m \quad (2.12)$$

Where,  $R$  is the radius of the filament,  $\%Porosity_l^m$  is the porosity of  $m^{th}$  pore cell area in  $l^{th}$  sub-region and  $L_{l,1}^m, L_{l,2}^m, L_{l,3}^m, L_{l,4}^m$  are the four arms of pore cell as shown in Fig. 4(b).

### 3 OPTIMUM TOOL PATH DESIGN

The proposed porous structure design provides a controllable and gradient porosity along the scaffold architecture. Even though some earlier researches put emphasis on the variational porosity design but fabrication techniques for those designs remains a challenge [10]. Therefore, an optimum tool path plan needs to be generated for the designed scaffolds.

#### 3.1 Tool-path plan for Sub-regions

The tool-path should be planned through inserted sub-regions arm,  $SA$  with minimum amount of over deposition, and start and stops. To generate the tool path for the first layer i.e. sub-region section layer, the sub-region arms need to bridge the medial region via the projected points  $bp'_l$  and connect with the sub-region arm from other side of medial axis as shown in Fig. 5. The idea is to develop the tool path between the point set  $P_{C_i}$  on the outer contour, crosshatches through the medial region and avoid or minimize any directional transition caused by that. The sub-region arms are then connected with the projected point set  $BP'$  to generate the tool-path.

The developed tool-path needs to start with a sub-region arm closest to the edge of the medial axis (Fig. 5) while initialization of tool-path on another location increases the number of discontinuity during deposition process. In addition, if the number of sub-region arm is odd, then tool-path should start from the external feature i.e. from point  $sp_l$ ; otherwise it should start from the other end point  $bp_l$  located on the medial contour to reduce or eliminate any possible discontinuity or jumps. This enables completion of connection and crosshatching between the sub-region arms with minimal jumps (if any) through the inner regions. Moreover, during the crosshatching through the medial region, the points set  $BP'$  are reevaluated and eliminated as  $BP' = BP' \cap bp'_c, bp'_b : |bp'_c bp'_b| \leq \delta/2 \quad \forall bp'_c \text{ and } bp'_b \in BP'$  and such elimination would increase the continuity during the deposition of sub-regions. The following algorithm describes the tool-path generation for layer 1.

#### Algorithm 1: Tool-path for sub-region layer (Layer 1)

**Input:** The point set  $SP = \{sp_l\}_{l=0,1..L}$ ;  $BP = \{bp_l\}_{l=0,1..L}$  and  $BP' = \{bp'_l\}_{l=0,1..L}$

**Out Put:** Consecutive organized point set  $OP = \{op_l\}_{l=0,1..T} : T \leq 3L$  for tool-path.

**Start:**

Initialize  $t \rightarrow 1$ ;

For  $i=0$  To  $L$

##### Initializing the Tool-path

If  $L \text{ Mod } 2 = 0$  then  $op_t \leftarrow bp_a$  and  $op_{t+1} \leftarrow sp_a$ ;

$BP = BP \cap bp_a$  and  $SP = SP \cap sp_a$ ;

$t \rightarrow t + 2$ ;

Calculate the  $sp_c \in SP : |sp_a sp_c| < |sp_a sp_d| \forall sp_d \in SP ;$   
 $op_t \leftarrow sp_c$  and  $op_{t+1} \leftarrow bp_c ;$   
 Elseif  $op_t \leftarrow sp_c$  and  $op_{t+1} \leftarrow bp_c ;$   
 End If;  
 $t \rightarrow t + 2 ;$   
 $SP = SP \cap sp_c$  and  $BP = BP \cap bp_c ;$   
**Tool-path along the medial region**  
 If  $|bp'_c bp'_b| \leq \delta / 2 \forall bp'_c$  and  $bp'_b \in BP'$  then  $op_t \leftarrow bp_b$  and  $op_{t+1} \leftarrow sp_b ;$   
 Elseif  $|bp'_c bp'_b| > \delta / 2 \forall bp'_c$  and  $bp'_b \in BP'$  then  $op_t \leftarrow bp'_c$  and  $op_{t+1} \leftarrow bp'_b ;$   
 $op_t \leftarrow bp_b$  and  $op_{t+1} \leftarrow sp_b ;$   
 End If;  
 $t \rightarrow t + 2 ;$   
 $BP = BP \cap bp_b$  and  $SP = SP \cap sp_b ;$   
 $BP' = BP' \cap bp'_c$  and  $bp'_b ;$   
**Connecting the Sub-regions arm for Tool-path**  
 If  $|sp_b sp_l| < 0 \forall sp_l \in SP$  then  $op_t \leftarrow sp_l$  and  $op_{t+1} \leftarrow bp_l ;$   
 Else  
 Calculate the  $sp_l \in SP$  so that  $|sp_b sp_l| < |sp_b sp_d| \forall sp_d \in SP ;$   
 $op_t \leftarrow sp_l$  and  $op_{t+1} \leftarrow bp_l ;$   
 End If;  
 $t \rightarrow t + 2 ;$   
 Next  
 Initialize  $j \rightarrow 1 ;$   
 For  $j = 0$  To  $T$   
     Connect Line between  $op_j op_{j+1}$   
 Next  
**End**

### 3.2 Deposition Path for Required Porosity

Due to the irregular geometry, the pore cell generating lines passing across the sub-regions do not necessarily have proper connections between them as shown in Fig. 4(a). These sub-region dividing lines are positioned in the consecutive layer to generate the desired and allowable pore size and to ensure both bio-logical and mechanical functionalities. To ensure the proper interpretation of the design objective during its fabrication, a feasible tool-path plan needs to be developed to minimize the deviation between designed and the fabricated structure. By connecting those lines consecutively without any transformation could generate stepped dominated tool path which might not be favorable for SFF-based fabrication systems. Besides such tool-path will generate material over-deposition and will restrict the permeability in the internal channel network. To ensure better continuity, an area weight based point insertion algorithm [9] is used as shown in Fig. 6(a). This algorithm generates a spiral like pattern along the scaffolding area. Finally after generating the deposition path for both

layers individually, they are combined together to make the continuous and interconnected tool path as shown in Fig. 6(b).

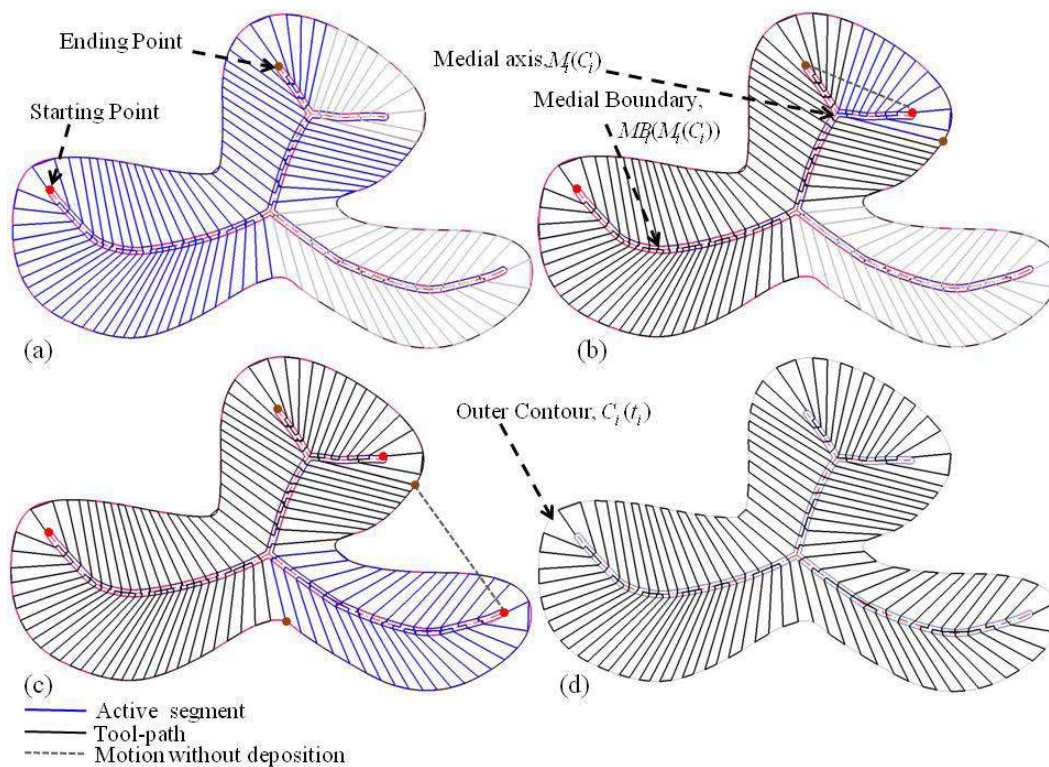


Fig. 5: Simulation of tool-path for the deposition through Sub-region 1 arm.

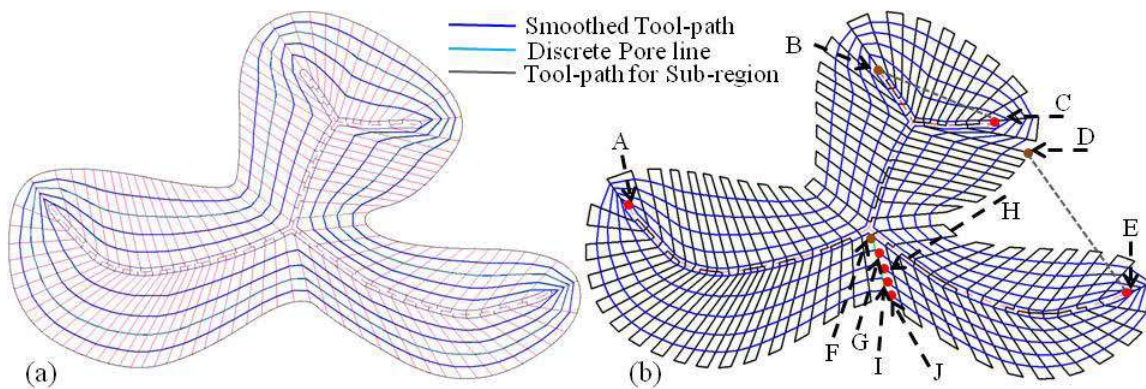


Fig. 6: (a) Smoothed pore generating tool-path (b) Final combined tool-path with start-ending sequence as A-B-C-D-E-F-G-H-I-J.

#### 4 IMPLEMENTATION

The proposed techniques have been implemented with a 2.3 GHz PCs using Rhino Script and Visual Basic programming languages on a sample femur bone slice extracted using ITK-Snap 1.6 [19] and Mimics Software[5]. The example femur slice is shown in Fig. 7. The porous structure is generated for variable but controllable porosity along its architecture with 50%-60%-70%-80%-90%-75%-60%-50% porosity from outer to inner region. A 150 micron filament diameter is used for deposition. Fig. 7 shows the generated medial axis and the corresponding medial boundary for the example. The scaffolding area has been discretized with 225 numbers of sub-regions which is accumulated from 2620 number of ruling lines. Sub-regions are divided into pore cells according to the corresponding porosity as shown in Fig. 8(b).

To generate the tool path, the lower widths of the sub-regions are decomposed on the medial axis with the methodology discussed in section 2.4. By following Algorithm 1, the sub-regions were connected through the medial region and the continuity has been achieved for the layer as shown in Fig. 9(b)-(f). A relatively smoother tool-path has been generated for the consecutive layer with the smoothing algorithm discussed earlier and the corresponding layer has been shown in Fig. 10.

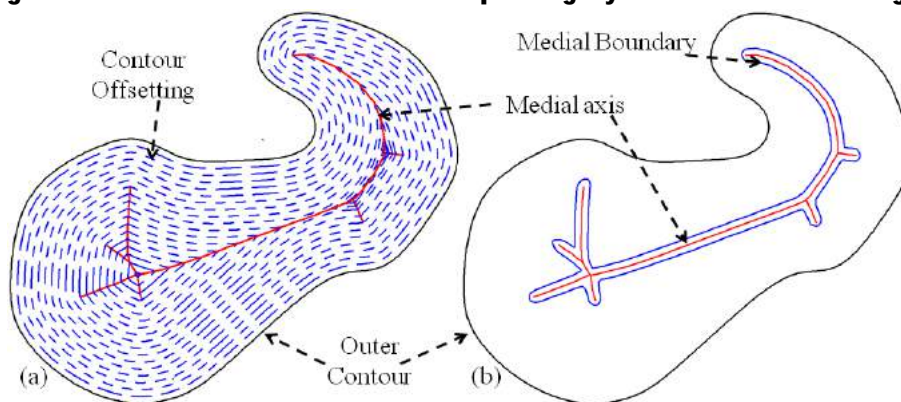


Fig. 7: (a) The medial axis (b) medial boundary formation.

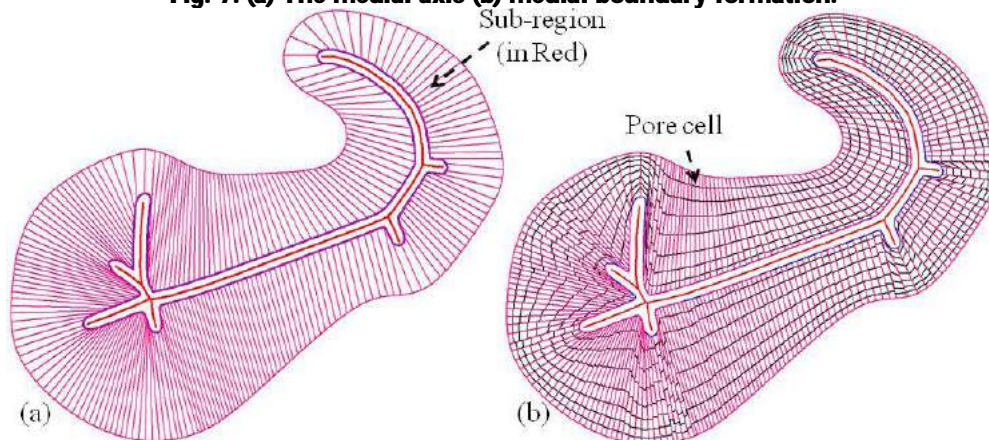


Fig. 8: (a) Sub-regions formation from the ruling lines (b) dividing sub-regions by generating desired area pore cell.

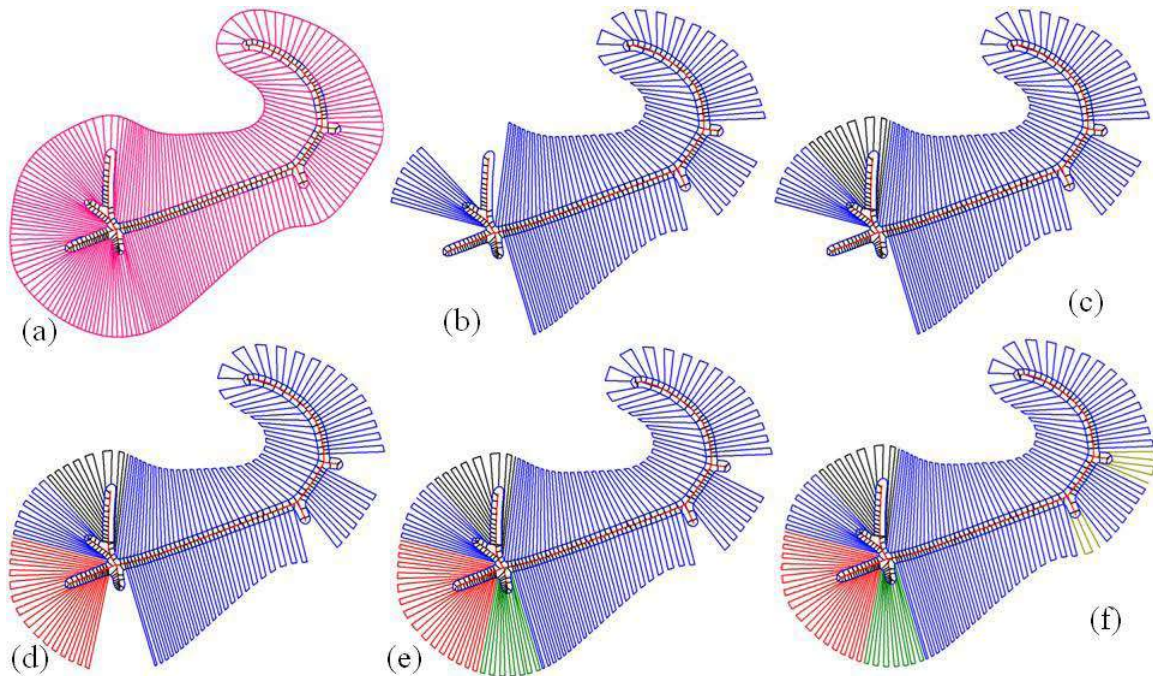


Fig. 9: (a) Decomposing of sub-region base on medial axis (b)-(f) Simulation of tool-path for the deposition through Sub-region  $\bar{N}$  arm.

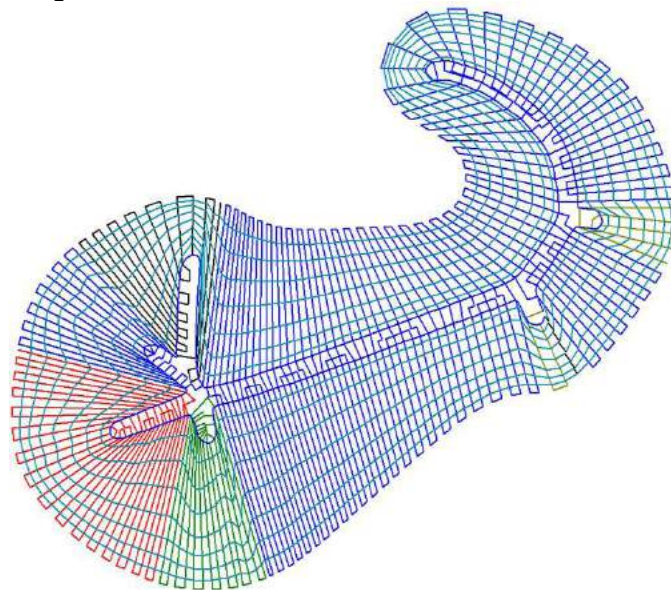


Fig. 10: Final combined tool-path for controllable porosity along its architecture with 50%-60%-70%-80%-90%-75%-60%-50% porous from outer to inner region.

For demonstration purpose, two consecutive slices of the femur example was fabricated with a 3D micro-nozzle biomaterial deposition system [9]. To fit into the working envelope of the fabrication system, the actual human femur model has been scaled down by 33%. In the fabricated model, a total

of 103 sub-regions have been used to discretize the scaffolding area. Each sub-region has been segmented with five equal area pore cells as shown in Fig. 11. The model has been fabricated with 250 micrometer substrate diameter.

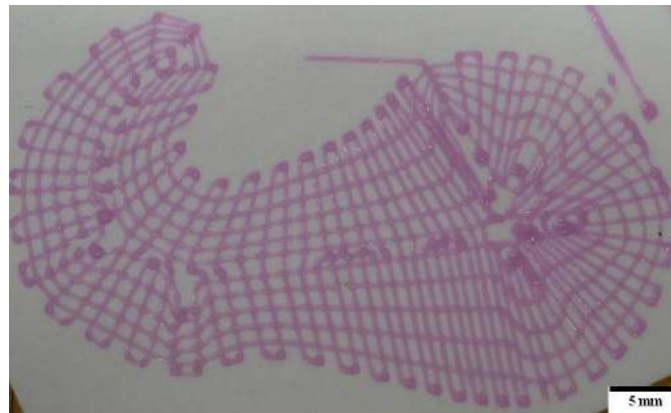


Fig. 11: Bio-fabrication of two consecutive for the femur slices with a constant porosity of 75%.

As shown in Figure 11, there are some material over depositions along the outer and inner edges. This is due to the sharp and sudden changes in the tool-path direction along the edge. Speeding up the process particularly in the edge could alleviate this over deposition but complete elimination would be a challenge for our current fabrication setup.

## 5 CONCLUSION

In this paper we developed a novel design methodology for controllable gradient porosity along the scaffold architecture. The developed design methodology ensures fabrication of the designed scaffolds using SFF based fabrication techniques. The controllable gradient porosity has been achieved by designing the two consecutive layers simultaneously. The first layer was designed with sub-regions while the consecutive layer was constructed with peripheral contours. And combination of these two layers generates pore cells with desired porosity. A feasible tool-path plan has been developed to fabricate the designed scaffolds structure. The tool path planning method generates interconnected and controlled pore size with desired accuracy along the scaffold architecture. The generated tool path plan can be used for SFF-based fabrication processes.

## REFERENCES

- [1] Adachi, T.; Osako, Y.; Tanaka, M.; Hojo, M.; Hollister, S. J.: Framework for optimal design of porous scaffold microstructure by computational simulation of bone regeneration, *Biomaterials*, 27 (21), 2006, 3964-3972. <http://dx.doi.org/10.1016/j.biomaterials.2006.02.039>
- [2] Blum, H.; Nagel, R. N.: Shape description using weighted symmetric axis features, *Pattern Recognition*, 10 1978, 167-180. [http://dx.doi.org/10.1016/0031-3203\(78\)90025-0](http://dx.doi.org/10.1016/0031-3203(78)90025-0)
- [3] Gaetani, R.; Doevendans, P. A.; Metz, C. H. G.; Alblas, J.; Messina, E.; Giacomello, A.; Sluijter, J. P. G.: Cardiac tissue engineering using tissue printing technology and human cardiac progenitor

- cells, *Biomaterials*, 33 (6), 2012, 1782-1790.  
<http://dx.doi.org/10.1016/j.biomaterials.2011.11.003>
- [4] Hollister, S. J.; Maddox, R. D.; Taboas, J. M.: Optimal design and fabrication of scaffolds to mimic tissue properties and satisfy biological constraints, *Biomaterials*, 23 (20), 2002, 4095-4103.  
[http://dx.doi.org/10.1016/S0142-9612\(02\)00148-5](http://dx.doi.org/10.1016/S0142-9612(02)00148-5)
- [5] <http://www.materialise.com/mimics>, *Mimics*, (Issue), ed 2008.
- [6] Hutmacher, D. W.; Schantz, J. T.; Lam, C. X. F.; Tan, K. C.; Lim, T. C.: State of the art and future directions of scaffold-based bone engineering from a biomaterials perspective, *Journal of Tissue Engineering and Regenerative Medicine*, 1 2007, 245-260. <http://dx.doi.org/10.1002/term.24>
- [7] Karande, T. S.; Ong, J. L.; Agrawal, C. M.: Diffusion in Musculoskeletal Tissue Engineering Scaffolds: Design Issues Related to Porosity, Permeability, Architecture, and Nutrient Mixing, *Annals of Biomedical Engineering*, 32 (12), 2004, 1728-1743. <http://dx.doi.org/10.1007/s10439-004-7825-2>
- [8] Khoda, A.; Koc, B.: Deformable Porosity for Multi-Functional Tissue Scaffolds, *ASME Transactions, Journal of Medical Device* (Submitted), 2011.
- [9] Khoda, A.; Ozbolat, I. T.; Koc, B.: A functionally gradient variational porosity architecture for hollowed scaffolds fabrication, *Biofabrication*, 3 (3), 2011, 1-15.  
<http://dx.doi.org/10.1088/1758-5082/3/3/034106>
- [10] Khoda, A. B.; Koc, B.: Designing Functional Porosity in Heterogeneous Bone Tissue Scaffolds with Variational Filament Modeling, *CAD* (Submitted), 2011.
- [11] Khoda, A. K. M. B.; Ozbolat, I. T.; Koc, B.: Engineered Tissue Scaffolds With Variational Porous Architecture, *Journal of Biomechanical Engineering*, 133 (1), 2011, 011001.  
<http://dx.doi.org/10.1115/1.4002933>
- [12] Lee, S.-H.; Shin, H.: Matrices and scaffolds for delivery of bioactive molecules in bone and cartilage tissue engineering, *Advanced Drug Delivery Reviews*, 59 (4-5), 2007, 339-359.  
<http://dx.doi.org/10.1016/j.addr.2007.03.016>
- [13] Levenberg, S.; Langer, R.: Advances in Tissue Engineering, in *Current Topics in Developmental Biology*. vol. Volume 61, P. S. Gerald, Ed., ed: Academic Press, 2004, 113-134.
- [14] Lin, C. Y.; Kikuchi, N.; Hollister, S. J.: A Novel Method for Biomaterial Internal Architecture design to match bone plastic properties with desired porosity, *Journal of Biomechanics*, 37 2003, 623-636. <http://dx.doi.org/10.1016/j.jbiomech.2003.09.029>
- [15] Liu, Y.; Zhu, F.; Zhu, H.: Review on Techniques of Design and Manufacturing for Bone Tissue Engineering Scaffold, in *Biomedical Engineering and Informatics, 2009. BMEI '09. 2nd International Conference on*, 2009, 1-4.
- [16] Ozbolat, I. T.; Koc, B.: Multi-directional blending for heterogeneous objects, *Computer-Aided Design*, 43 (8), 2011, 863-875. <http://dx.doi.org/10.1016/j.cad.2011.04.002>
- [17] Sobral, J. M.; Caridade, S. G.; Sousa, R. A.; Mano, J. F.; Reis, R. L.: Three-dimensional plotted scaffolds with controlled pore size gradients: Effect of scaffold geometry on mechanical performance and cell seeding efficiency, *Acta Biomaterialia*, 7 (3), 2011, 1009-1018.  
<http://dx.doi.org/10.1016/j.actbio.2010.11.003>

- [18] Tay, C. Y.; Irvine, S. A.; Boey, F. Y. C.; Tan, L. P.; Venkatraman, S.: Micro-/Nano-engineered Cellular Responses for Soft Tissue Engineering and Biomedical Applications, *Small*, 7 (10), 2011, 1361-1378. <http://dx.doi.org/10.1002/smll.201100046>
- [19] [www.itksnap.org](http://www.itksnap.org), ITK-SNAP, in 1.6(Issue), ed 2008.